Bioprinting 50 (2025) e00432

Contents lists available at ScienceDirect

Bioprinting

journal homepage: www.sciencedirect.com/journal/bioprinting

Reseach paper

Dual-crosslinkable gallol bioinks via pH-controlled oxidation and photocrosslinking with enhanced shear thinning and viscoelastic behavior

Hatai Jongprasitkul [a,b], Sanna Turunen [a,c], David A. Fulton [b], Minna Kellomäki [a], Vijay Singh Parihar [a,*]

[a] Biomaterials and Tissue Engineering Group, Faculty of Medicine and Health Technology, Tampere University, 33720, Tampere, Finland
[b] Chemistry-School of Natural Science and Environmental Sciences, Newcastle University, Newcastle-upon-Tyne, NE1 7RU, UK
[c] New Materials and Processes Research Group, Faculty of Engineering, Turku University of Applied Sciences, 20520, Turku, Finland

ARTICLE INFO

Keywords:
Bioprinting
Injectable hydrogels
Gallol-based biomaterials
Hyaluronic acid
Photocrosslinking
Dual crosslinking

ABSTRACT

Our research work proposes a dual crosslinking approach to address the limitations of the gallol-mediated auto-oxidation approach in bioprinting, where rapid oxidative crosslinking can cause premature gelation, leading to clogging or printing failure. We enabled a gallol hydrogel ink to be printable via extrusion-based 3D bioprinting by utilizing its temporal shear-thinning properties. By raising the pH level, interactions between gallol-modified hyaluronic acid methacrylate (HAMA-GA) can be triggered to form a weak hydrogel. This feature provides injectability and extrudability for the hydrogels. Subsequent photocrosslinking results in indefinite oxidative crosslinking. The oxidative coupling in HAMA-GA was partially inhibited by UV light during the photo-crosslinking step. As a result, the printed hydrogel formed a dual-crosslinked network containing both oxidative and photo-induced bonds, which contributed to enhanced structural stability over time. Our proposed approach addresses the challenges of gallol-mediated oxidation, including overgelation that hinders extrusion in 3D bioprinting, offering a promising solution for improved printability and shape fidelity. HAMA-GA ink was bioprintable at pH 5.5 using an extrusion-based 3D printer, showing cytocompatibility (~95 % viability). This strategy is valuable for designing hydrogel inks with tunable properties for 3D bioprinting while maintaining tissue adhesive properties of gallol moieties.

1. Introduction

The utilization of bioprinting is expanding across various fields, including basic tissue engineering, regenerative medicine, personalized medicine, and organ-on-chip technology [1]. Bioink, a crucial component of bioprinting, plays a significant role in fabricating suitable 3D scaffolds which are essential for creating more physiologically relevant *in vitro* models [2]. An optimal bioink should exhibit desired physicochemical properties, encompassing appropriate mechanical, rheological, chemical, and biological characteristics [3]. The choice of printing technique relies on factors such as the biopolymers used, the crosslinking chemistry of the bioink, and the size and complexity of the intended scaffold [4]. In addition, the utilization of injectable hydrogels is expanding in applications from basic tissue engineering to organ-on-chip technology. Injectable hydrogels can temporarily adapt under stress and subsequently restore their original properties due to their self-healing properties [5]. The combination of injectability and self-healing properties in hydrogels offers high tunability for precise delivery with a narrow syringe [6].

In recent years, the introduction of mussel-inspired gallol moieties into bioink formulations has opened new possibilities in 3D bioprinting [7–10]. For instance, during *in situ* bioprinting in wound dressing, the presence of body fluids can complicate the surgical procedure, making wet adhesive properties of gallol-based bioinks crucial for effective wound sealing in wet conditions. These aromatic rings with three hydroxyl groups have been used in bioink development, such as the synthesis of gallol-modified hyaluronic acid (HA-GA) and gelatin-gallol (GEL-GA) by Shin et al. [11,12] These polymers form a gel via non-covalent hydrogen bonding interactions between gallols and protein backbones and undergo gradual covalent crosslinking facilitated by a spontaneous oxidation mechanism [12,13]. Another exciting development is the newly introduced bioink obtained from chitosan (CS) and gallic acid (GA) by Gwak et al. [14,15] The 3D printed scaffolds demonstrated remarkable shape accuracy, coupled with the

* Corresponding author.
E-mail address: vijay.parihar@tuni.fi (V.S. Parihar).

https://doi.org/10.1016/j.bprint.2025.e00432
Received 17 May 2025; Received in revised form 24 July 2025; Accepted 11 August 2025
Available online 14 August 2025

optimization of various printing parameters. The CS-GA hydrogel showed rapid formation under physiological pH conditions, eliminating the need for chemical crosslinking agents [14].

The integration of bioadhesive technologies inspired by mussel chemistry into bioprinting, has gained significant attention. However, numerous limitations have been reported with the gallol-mediated auto-oxidation approach, as existing literatures consistently highlight the challenge of controlling oxidative crosslinking [12,16]. These limitations include time-dependent oxidative crosslinking, leading to continued oxidation until maximum crosslinking is reached, which may disrupt tissue-adhesive properties due to the presence of *o*-quinones derived from the catechol ring. Moreover, the rapid oxidative crosslinking observed in gallol-functionalized polymers leads to a narrow printability window of less than 30 min, providing practical difficulties during printing [11,12]. To overcome these challenges, particularly the need for rapid stabilization in applications such as injectable hydrogels and bioinks, photocrosslinking is often incorporated to provide controlled crosslinking. This method improves fabrication flexibility, enabling rapid hydrogel stabilization upon UV exposure. Additionally, we leveraged the responsive interactions within HAMA-GA to form a weak hydrogel through pH elevation. Subsequently, the use of UV light inhibited the oxidative crosslinking of the gallol moieties while also forming covalent bonds, which stabilized the hydrogel structure. In addition, we balanced the adhesive and cohesive forces of the photo-crosslinkable gallol biomaterial ink. Rheological characterization was performed to study the material in both pre- and post-photocrosslinking, providing insights into the combined roles of oxidative crosslinking in gallol moieties and covalent bonding after photocrosslinking.

2. Materials and methods

Hyaluronic acid (HA, MW 100 kDa) was purchased from Lifecore Biomedical (Chaska, USA). Methacrylic anhydride (MA), gallic acid (GA, 3,4,5-trihydroxy benzoic acid), hydrazine hydrate, 1-ethyl-3-(3-dimethyl aminopropyl)-carbodiimide hydrochloride (EDC), 1–hydroxy benzotriazole hydrate (HOBt), dimethyl sulfoxide (DMSO), and Irgacure 2959 (I2959) were purchased from Merck KGaA, Darmstadt, Germany. Dialysis membranes used for purification were purchased from Spectra Por-6 (MWCO 3500). DI water (deionized water, Miele Aqua Purificator G 7795, Siemens) was used. Dulbecco's phosphate-buffered saline (DPBS) was prepared in the lab. All solvents were of analytical quality. ^{1}H NMR analysis was carried out on an NMR spectrometer (SCZ500R, JEOL Resonance, Japan). Dulbecco's modified Eagle's medium (DMEM), Dulbecco's modified Eagle's medium/F-12, fetal bovine serum (FBS), penicillin−streptomycin−amphotericin B solution (P/S) and Dulbecco's Phosphate-Buffered Saline (DPBS) and live/dead assay kits (488/570) were purchased from Fisher Scientific Oy, Finland. Human dermal fibroblasts (HDFB, P2, cell density of 5×10^5/mL) were purchased from Thermo Fisher Scientific, USA. All chemicals and reagents used were of analytical grade. All solutions were prepared with deionized (DI) water.

Synthesis and characterization of gallol-modified hyaluronic acid methacrylate (HAMA-GA) The synthesis and characterization of HAMA are described in SI (Figure S-1). As described in the previous studies, HAMA-GA was prepared through EDC coupling reactions [17,18]. In brief, HAMA (400 mg) was dissolved in DI water (75 mL). HOBt (153 mg, 1.0 equiv.) was added to the HA solution, and stirring was continued until a homogeneous mixture was achieved. Gallic hydrazide (GH, 184 mg, 1 equiv.; synthesis details provided in SI Figure S-2) was dissolved separately in DMSO (25 mL). The GH solution was then added dropwise to the previously prepared reaction mixture while maintaining the pH at 4.75 using 1 M HCl and 1 M NaOH. EDC (184 mg, 1 equiv.) was added according to the 20 % modification degree of GA in HAMA and reacted overnight. The solution was then dialyzed against dilute HCl (pH = 3.5) containing 100 mM NaCl (6 × 2L, 48 h) to remove unreacted EDC and HOBt using dialysis membranes. The final white fluffy product was obtained after freeze-drying. ^{1}H NMR spectroscopic analysis was used to quantify the degree of modification of GA in HAMA by observing the presence of a distinctive aromatic peak at 6.99 ppm of GA, and the degree of modification was determined to be around 20 %. Fourier-transform infrared (FTIR) spectra were collected using the ATR method on a PerkinElmer Spectrum One spectrophotometer (PerkinElmer, Waltham, MA). Freez-dried samples were pressed onto the ATR crystal, with spectra recorded at 4 cm^{-1} resolution, averaged over 16 scans from 4000 to 400 cm^{-1}

Biomaterial ink formulations The lyophilized HAMA-GA (5 % w/v) was dissolved in DBPS containing photoinitiator (I2959, 0.5 % w/v) at 37 °C and stirred until fully dissolved. The initial pH of the HAMA-GA precursor was 3.5, which was designated as the first ink formulation (HAMA-GA pH 3.5). The first ink formulation was then stored at 37 °C for 30 min to remove air bubbles before proceeding to the next formulation. The second ink formulation aimed to adjust the pH of HAMA-GA to 5.5 (HAMA-GA pH 5.5), while the third ink formulation aimed to adjust the pH of HAMA-GA to 7 (HAMA-GA pH 7). The pH of the second and third formulations was adjusted by adding 0.1 M NaOH dropwise and vigorously stirring until the desired pH was reached. Each ink formulation was subjected to three incubation time points: 0, 15, and 30 min. Following incubation, the ink formulations were evaluated for oxidative crosslinking over time and flow behavior using a rotational rheometer (Discovery HR-2, TA Instruments Inc., USA). After pre-screening via rheology, the ink formulations were selected for 3D printing, following all the protocols from previous studies [18–21].

The gelation kinetics of oxidative crosslinked HAMA-GA inks To further understand the gelation kinetics, an ultraviolet–visible (UV–vis) spectrophotometer (Shimadzu UV-3600 plus UV–VIS–NIR spectrophotometer) and a rotational rheometer were used to analyze the pH/time-dependent oxidative crosslinking in HAMA-GA inks. All measurements were carried out in triplicate.

For rheological testing, the instrument was equipped with parallel plate geometry. The gap between the plate and geometry was set at 2.5 mm, and the measurement was performed at RT. The gelation kinetics of time and pH-dependent oxidative crosslinking were measured in frequency and time sweep. The established protocols were based on previous works [17–21], where the frequency sweep was utilized to determine the sol and gel states of the samples, while the time sweep was employed to observe gelation time. Both protocols were performed to investigate the viscoelastic behavior of the inks by determining the storage (G′) and loss (G″) moduli. The sol and gel states were distinguished by comparing the G′ and G″ values as follows: G" > G′ indicated a sol state, G" = G′ indicated a sol-gel transition, and G" < G' indicated a gel state [17]. The frequency sweep was conducted over a range of 0.1–100 Hz while maintaining a constant strain of 0.1 %. The time sweep was observed for a duration of 7000 s, with the frequency set at a constant of 1 Hz and the strain maintained at 0.1 %. For the gelation time of photocrosslinking, *in situ* photorheology was performed using a time sweep for 400 s, during which UV light (wavelength of 365 nm, intensity of 25 mW/cm^2, BlueWave 50 UV curing spot lamp, DYMAX Corp., USA) was activated at 100 s.

To monitor the formation of *o*-quinone during oxidative crosslinking in HAMA-GA, analysis was performed using a UV–vis spectrophotometer (350−700 nm). Each sample was prepared at a concentration of 0.5 % w/v across the pH range of 3–7 by adding 0.1 M NaOH and transferring it into a quartz cuvette. To investigate the photo-inhibition effect of HAMA-GA, the oxidized samples (pH > 5) were irradiated with UV light for 2 min and measured in a similar fashion.

Flow behavior and 3D printing of HAMA-GA hydrogels The flow behavior of the biomaterial inks was also assessed through rheological measurements at room temperature (RT). The samples underwent a shear rate sweep ranging from 0.1 to 100 s^{-1} to measure viscosity over the range of shear rate. If the sample escaped from the geometry due to over-gelation, the instrument was adjusted to perform oscillatory measurements with frequency sweep to measure complex viscosity over the

angular frequency range of 0.1–100 rad/s. Shear thinning properties of the inks were obtained from viscosity curves. For critical strain measurement, the experiment was conducted using an amplitude sweep test with a strain ranging from 0.1 to 1000 % while maintaining frequency at 1 Hz.

Printability assessment and 3D bioprinting of HAMA-GA inks The pre-screened formulations were selected for multi-layered grid printing using an extrusion-based 3D printer (Brinter® One, Brinter Ltd, Finland). The 3D printer was equipped with a standard pressure-driven control printhead and a UV light control module. The selected ink was slowly transferred to a UV-shielded 10 mL cartridge attached with a 250 μm standard plastic tapered nozzle. The ink was printed onto a glass slide at RT using a printing speed of 6 mm/s. The pressure was adjusted until a uniform fiber was extruded from the 25G nozzle. Subsequently, the fiber width and printed constructs were captured using a mirrorless camera and an optical microscope. These images were then analyzed using image processing software (ImageJ). The printing parameters were readjusted before each printing session, which included z-height calibration, dispensing of photocrosslinked ink on the nozzle tip, and adjusting the printing pressure.

According to our previous works, the pre-screening of fiber quality was evaluated to ensure the coherent fiber formation (in the air) at each ink candidate: droplet, smooth and irregular fiber [21,22]. After printing, the fiber deposition on the glass slide substrate was evaluated by measuring the fiber width relative to the nozzle size, providing an assessment of the printing resolution [23]. After that, printability (PR) was determined based on established methods [24], which involved assessing the squareness of pores within the printed grid structure. The 20 mm × 20 mm grid model with 15 % filling density was utilized as the standard grid model for PR value calculation. The PR value equal to 1 indicates a perfectly square shape, resulting in high printing resolution, while PR < 1 indicates a circular shape and PR > 1 indicates an irregular shape. PR values lower or higher than 1 often result in poor printing resolution.

The oscillatory measurements and swelling studies of dual crosslinked HAMA-GA hydrogels HAMA-GA samples at pH 3.5, 5.5, and 7 were cast into a mold, then divided into two sets of hydrogels: plain oxidative crosslinked and dual crosslinked hydrogels. For plain oxidative crosslinked samples, casted HAMA-GA samples were incubated overnight at 37 °C, whereas dual crosslinked samples were irradiated under UV light for 2 min (365 nm in wavelength and the intensity of 25 mW/cm^2). All casted hydrogel samples were subsequently subjected to viscoelasticity measurement and swelling studies.

The viscoelasticity of hydrogels was measured at RT under frequency (ranging from 0.1 to 100 Hz, constant strain at 0.1 %) and amplitude sweep ranging from 0.1 to 100 %, constant frequency at 1 Hz). The results were analyzed to determine G′ and G″ in the linear viscoelastic region (LVR) and critical strain, which represents the breaking point to evaluate the improvement of viscoelasticity at the end of the LVR.

The swelling studies were performed to investigate the stability of oxidative and dual crosslinked hydrogels. All hydrogels were immersed in 0.1 M phosphate-buffered saline (PBS) solution. The hydrogels were maintained at 37 °C ± 0.5 °C in a shaking incubator at 90 rpm until various time points (0, 1, 2, 3, 5, 7 and 15 d). The casted hydrogels were weighted after fully crosslinked in each crosslinking method and designated as zero time point and initial weight (W_0). At a specific time, the hydrogel samples were removed and gently blotted with filter paper to remove the residual solution and weighted as W_s. The swelling ratio was calculated as W_s/W_0.

Adhesiveness of HAMA-GA hydrogels A tack test was performed for oxidative and dual crosslinked HAMA-GA hydrogels using a rotational rheometer. The bioadhesion of hydrogels (n = 5, for each parameter) was investigated using *in situ* photocrosslinking and adhesiveness in the axial direction. This established method has been previously described in another study [17,25,26]. In brief, circular sheets of porcine muscle with a diameter of 12 mm were carefully prepared and glued between the geometry and the bottom plate. Subsequently, the HAMA-GA ink was cast into a 2.5 mm gap between two tissue sheets (upper and bottom plates) and allowed to oxidize for 30 min. For dual-crosslinking samples, UV light irradiation was conducted for 2 min to crosslink the sample. Following this, the geometry was lifted in axial motion at a constant rate of 20 μm/s, and the change in axial force was recorded upon detachment. An axial force curve was then fitted to observe the impact of photocrosslinking on the adhesive properties of the hydrogel in comparison to plain oxidative crosslinking.

Cell laden bioprinting and cell viability HAMA-GA bioinks were prepared in DI water (pH ~3.5) and DPBS (pH ~5.5 or 7). Prior to printing or casting, the precursor solutions were mixed at a 1:1 vol ratio with cell suspension (2×10^6 cell density/mL) in DMEM, resulting in a final bioink with adjusted pH closer to physiological conditions. Immediately after photocrosslinking, constructs were immersed in complete culture medium to ensure restoration of a neutral environment. For cell studies, all materials and equipment were sterilized by UV irradiation for 30 min. All cell cultures were maintained in a cell culture incubator at 37 °C with 5 % CO_2. Prior to preparing the cell-laden hydrogels, HDFBs were cultured in DMEM supplemented with 10 % FBS and 1 % P/S. Once the cells reached confluency in the flask, they were resuspended in HAMA-GA bioink formulation. A live/dead staining assay was performed using the Live/Dead Cell Imaging Kit (488/570), following the manufacturer's instructions. Briefly, the DMEM was removed from the printed constructs. A working solution was then added, and the samples were incubated in the dark for 20 min. Imaging was performed using a fluorescence microscope (a Nikon Eclipse Ts 2) with a 10 × objective lens. Cell viability was determined by calculating the percentage of live cells (green) relative to the total number of cells (green and red). A minimum of six randomly selected images were analyzed using ImageJ software (n = 6 different spots on three constructs). Cells that stained both red and green were not counted as live cells.

Statistical analysis All results were presented as the mean ± standard deviation (SD). Statistical analysis was performed by MS Excel using one-way and two-way analysis of variance (ANOVA) with Bonferroni Post hoc test.

3. Results and discussion

The dual-or multi-crosslinking systems in hydrogels have been explored widely, which combine the advantage of crosslinking mechanism for enhanced hydrogel properties. For example, gelatin-gallol systems typically harness gelatin's inherent thermosensitivity (for physical gelation) or its modifiability with methacrylates (for photocrosslinking), alongside gallol properties for oxidative crosslinking, offering a versatile platform derived from an animal protein [11,20]. Similarly, chitosan-gallol systems utilize chitosan's positive charge for ionic gelation or its chemical reactivity for photo-crosslinking, in conjunction with gallol-mediated oxidative bonds, often resulting in robust polysaccharide-based hydrogels [14]. The advantages of each previously reported gallol based hydrogel are summarized in Table S1. Our study introduces a novel HAMA-GA system, which distinguishes itself from other gallol-modified systems by integrating the excellent biocompatibility and native ECM properties of hyaluronic acid with both photo- and oxidative crosslinking, providing unique advantages in terms of gelation kinetics, printability, mechanical behavior, and cytocompatibility.

HAMA-GA ink formulations and their gelation kinetics The synthesis of HAMA-GA is shown in Fig. 1A. HAMA was prepared through the reaction of HA with methacrylic anhydride to obtain the methacrylated polymer with the modification degree of 30 % of the disaccharide repeating units as determined by ^{1}H NMR spectroscopic analysis (Figure S-3-A). The modification degree was determined by integrating the olefinic peaks of the methacrylate group at $\delta = 6.12$ and 5.68 ppm and comparing this value to the methyl peak of the N-acetyl group of HA

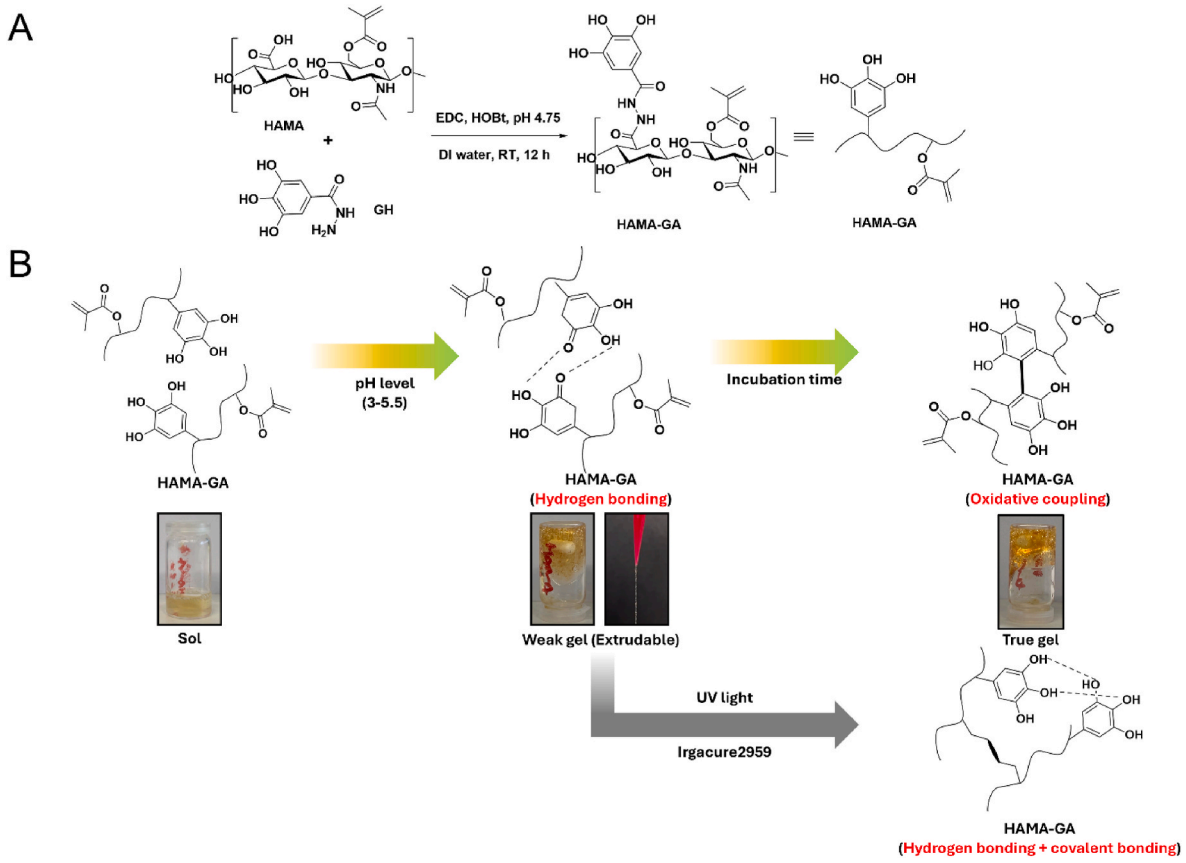

Fig. 1. Design approach for the biomaterial ink (HAMA-GA) and the effect of pH variation (3.5–5.5). (A) The synthesis route of HAMA-GA involves a carbodiimide coupling reaction between HAMA and gallic acid hydrazide (GH). (B) The effect of temporal oxidation on the printability window. Initially, hydrogen bonding is formed, but with extended incubation, it transitions to covalent bond due to oxidative crosslinking. Exposure to UV light quenches oxidative coupling formation while simultaneously forming irreversible covalent bonds to stabilize the hydrogel.

at $\delta = 1.95$ ppm. Subsequently, HAMA was subjected to gallol conjugation to achieve 20 % modification degree of gallol upon the HAMA backbone (HAMA-GA). The degrees of modification of GH were also determined by ^{1}H NMR spectroscopy (Figure S-3-A, merged in HAMA-GA figure). Confirmation of GH conjugation in HAMA was achieved through the observation of distinct peaks at $\delta = 6.98$ and 7.40 ppm, corresponding to the aromatic protons of GH (Figure S-3-B).

In general, the gallol group oxidizes to a quinone structure under highly basic conditions. The degree of oxidation of the gallol group is significantly influenced by the pH level and incubation time [17,18,27]. From previous studies, gallol-modified HA cannot form a true hydrogel due to insufficient levels of polymer modification, which limits oxidative crosslinking between the polymer chains [11,18]. Shin et al. achieved sufficient levels of intermolecular interaction to drive hydrogel formation by combining gallol-modified HA with gallol-modified gelatin [12]. However, our HAMA-GA formulation exceeded a 20 % degree of modification, enabling oxidative crosslinking from a sol to a gel state under the influence of pH levels and incubation time [18]. In our system, the oxidative crosslinking exhibited time-dependent properties ranging from short-term crosslinking, where hydrogen bonding primarily facilitates interactions between polymer chains, resulting in weakly extrudable hydrogels, to long-term crosslinking, where gallol oxidation drives covalent crosslinking, forming true hydrogels through oxidative coupling of gallols (Fig. 1B). In addition, further increases in pH to 7 and basic (7.5–8) or prolonged incubation time resulted in instant true hydrogels because the oxidative coupling forms efficiently under basic conditions, which cannot be used for bioprinting. Our findings of oxidative crosslinking in gallol-functionalized polymers align with previous studies on gallol-modified gelatin and hyaluronic acid, where the crosslinking occurred to form true hydrogels over time. Subsequently, we hypothesize that application of UV light may serve as both a triggerable crosslinking system and a potential means to suppress oxidative coupling of gallols and *o*-quinone formation.

To further analysis of oxidative coupling of gallol based bioinks, FTIR spectroscopy was employed to investigate the oxidation (quinone formation) and oxidative coupling of gallic acid in HAMA-GA bioinks under varying pH conditions. The spectra of native HA, HAMA-GA, and HAMA-GA samples treated at pH 3.5, 5.5, 7, and 8 are shown in Fig. 3. The spectral region between 3000 and 3700 cm^{-1} shows a broad band attributed to O–H stretching vibrations, which is particularly important for confirming the presence of phenolic hydroxyl groups introduced through gallic acid conjugation. In the native HA spectrum, this band appears relatively weak and narrow, reflecting only the intrinsic hydroxyl groups in the polysaccharide backbone. Notably, the intensity and broadness of this O–H band vary with pH. At pH 3.5, the O–H stretch is especially intense and broad, suggesting that the phenolic groups remain largely unoxidized and that quinone formation is minimal. At pH 5.5, the peak becomes narrower and less intense, indicating the oxidation of phenolic groups to quinones. However, at pH 7 and 8, the peak broadens and intensifies again, due to the onset of oxidative coupling, which regenerates phenolic hydroxyl groups and contributes to the formation of polyphenolic networks or crosslinked structures. The broadened O–H region at higher pH may also partially reflect the reduction of quinones back to phenols during coupling.

The 1600–1700 cm^{-1} region corresponds to C=O stretching vibrations, characteristic of quinone groups. This region is relatively featureless in native HA. In contrast, HAMA-GA at pH 3.5 shows a clear but moderate peak, indicating early-stage quinone formation. At pH 5.5,

7, and 8, the C=O peak becomes more intense and broader, confirming enhanced oxidation of phenolic groups. At pH 8, the peak intensity is comparable to that at pH 7, suggesting a balance between ongoing quinone formation and oxidative coupling, which also contributes to the observed increase in the O–H region. Additional spectral features in the fingerprint region (1000–1500 cm^{-1}) support the presence of GA-related aromatic structures, with variations in peak shape and intensity reflecting pH-dependent structural transformations in the HAMA-GA network.

To study the crosslinking kinetics of oxidative crosslinking and photocrosslinking of HAMA-GA, the rheological characterization was monitored using a time sweep (Fig. 2A). All samples at pH 3.5 to 5.5 behaved as viscoelastic fluids at the zero-time point, designated as a sol state, displaying G" > G′, and exhibiting Newtonian fluid behavior as shown in Fig. 2A and B. Moreover, the sample at pH 3.5 did not exhibit a sol-gel phase transition until the end of observation, suggesting the gallol did not initiate significant hydrogen bonding under these conditions [28–30] because oxidation of GA did not occur at acidic pH. In contrast, the oxidization of HAMA-GA at pH 5.5 initially provided weak viscoelasticity, with G′ being greater than G″ but G′ gradually increased over time. In addition, the results (Fig. 2A) revealed that the ink at pH 7 showed immediate gelation to a gel state (G' > G″). The formation of the quinone form and subsequent oxidative crosslinking were also investigated using UV–vis spectroscopy [31]. Fig. 2B also confirmed the different phases of hydrogels under different pH conditions. Specifically, the pH 3.5 samples exhibited behavior consistent with the Maxwell viscoelastic model, as evidenced by the observed crossover point in the frequency sweep. In contrast, pH 5.5 and 7 samples behaved more like viscoelastic solids (G' > G") [32]. Fig. 2C demonstrates that the degree of oxidation in the gallol groups varies with pH levels, ranging from acidic to basic, where the *o*-quinone peak was observed within the absorption range of 400–500 nm. The intensity of the peak increased with higher pH levels.

Photo-inhibition effect of photocrosslinked HAMA-GA hydrogels In general, the process of oxidative crosslinking, driven solely by the formation of *o*-quinone and its subsequent dimerization, either through changes in pH or during incubation, leads to the creation of irreversible covalent bonds [11,12]. This process reduces the cohesive force within the hydrogel, ultimately leading to brittleness [33]. In this study, we functionalized the gallol system with methacrylate groups which enable photocrosslinking and provide flexibility in controlling gelation time, as shown in Fig. 2D. Each sample was cured with UV light for 300 s. During the first 100 s, the samples were in a pre-photocrosslinked state (before UV exposure), with distinct rheological properties observed at different pH levels. At pH 3.5, the low storage modulus (G′) indicated a sol state, while at pH 5.5, a sol-gel transition occurred, and at pH 7, the system formed a gel. After photocrosslinking, a covalent network was established through the reaction of methacrylate groups, which further contributed to the pre-crosslinking state at each pH level. It was observed that as the pH increased, the photocrosslinking rate decreased, as evidenced by the minimal change in G′ after UV exposure. This reduction in photocrosslinking efficiency was attributed to the restricted movement of the polymer network caused by the formation of oxidative crosslinking prior to photocrosslinking. In addition, photocrosslinking effectively quenched the oxidative crosslinking over time (Fig. 1) and induced a photo-bleaching effect, shifting the intense brown color of oxidation to a more

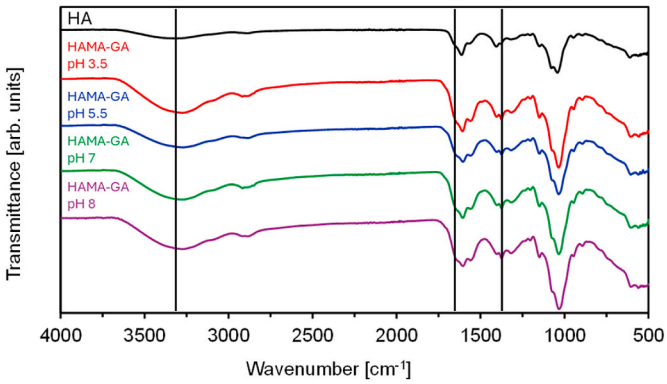

Fig. 3. FTIR spectra of native HA and HAMA-GA at various pH values (3.5, 5.5, 7 and 8). The spectral changes highlight pH-dependent shifts in chemical structure associated with gallol oxidation and crosslinking behavior.

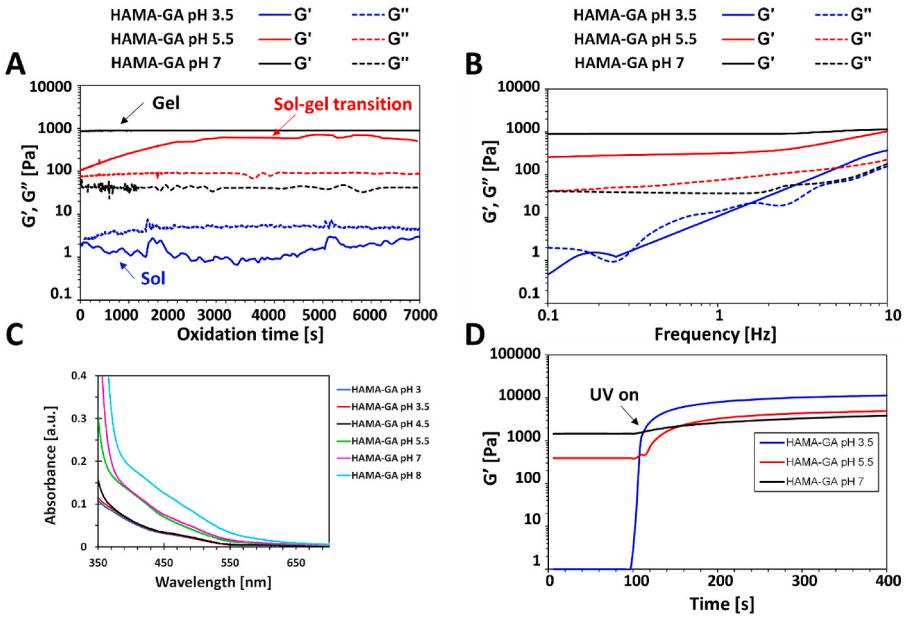

Fig. 2. Gelation kinetics of oxidized HAMA-GA ink at different pH levels, over time, and under photocrosslinking conditions. (A) Time-dependent moduli of oxidative crosslinking in HAMA-GA at pH 3.5, 5.5, and 7. (B) Viscoelasticity of HAMA-GA at pH 3.5, 5.5, and 7 at zero-time point, varying degrees of oxidation, measured by frequency sweep. (C) UV–vis spectra illustrating pH-induced oxidative crosslinking. (D) Gelation of HAMA-GA via photocrosslinking, demonstrating the successful integration of methacrylate and gallol groups in a single ink.

transparent color, as shown in Fig. 4A. The color intensity of gallol molecules increases with rising pH levels. However, after UV light exposure, the color reverts almost to its original tone. We also observed the photobleaching effect upon photocrosslinking due to the radical quenching phenomena in the presence of the photoinitiator [34]. This effect is also presumed to be influenced by the antioxidant properties inherent in gallol-based molecules and the oxygen inhibition effect in free-radical polymerization as we describe as the photo-inhibition effect [30,35]. Similar radical-inhibiting behavior of gallol and catechol groups has been observed in other hydrogel systems as well [36]. The results were confirmed by UV–vis spectroscopy, as evidenced by the reduction in the peak of *o*-quinone in the oxidized gallol group at pH 7 and 8 after UV light exposure, as shown in Fig. 4B.

Flow behavior and printability assessment and 3D printing of HAMA-GA inks The flow behavior of the biomaterial ink at pH 3.5, 5.5 and 7 was pre-characterized using a rotational rheometer to ensure appropriate viscosity and shear-thinning properties. Shear-thinning modulation induced by oxidative crosslinking processes modulate shear thinning properties, was accomplished through pH adjustment, increasing from 3.5 to 5.5. In Fig. 5A, the ink at pH 5.5 demonstrated high shear-thinning behavior on a short-time scale (15 min incubation time), displaying a decrease in complex viscosity as the angular frequency increased (from 0.1 to 100 rad/s). This behavior can be explained by the Cox-Merz rule, suggesting that the inks behaved like a weak gel state, as the gel tended to escape from the geometry under high centrifugal force [7]. These results were consistent with our previous studies on HAGA-HAMA blend biomaterial inks, where gallol-based polymers exhibited shear-thinning properties when oxidative crosslinking occurred among the gallol moieties at higher pH values [18]. Similarly, the result of oxidative crosslinking is in accordance with the narrow printability window due to the rapid oxidation of gallol moieties in the presence of oxidative coupling formation at basic pH [12]. However, the ink at pH 7 was unsuitable for printing because it immediately transitioned to a gel state, further narrowing the printability window. Additionally, the sample completely escaped from the geometry at high stress, as shown in Fig. 5B. In comparison, samples at pH 5.5 maintained their cohesive force. They exhibited reduced storage moduli, while the samples at pH 3.5 did not change in viscosity (Fig. 5A) or storage moduli (Fig. 5B), regardless of the increase in angular frequency.

HAMA-GA at pH 5.5 was selected to be printed via an extrusion-based bioprinter. A time-dependent printability window was also established by printing the ink into multi-layered grid structures (Fig. 5C). In detail, the ink with zero incubation time exhibited a watery-like behavior, producing droplets that spread upon deposition on the printing bed. In contrast, an incubation time of 15 min provided smooth and consistent filament formation, representing the optimal incubation time. However, when the incubation time reached 30 min or more, the filament began to crosslink further, becoming irregular and prone to frequent nozzle clogging. The printed structures were photocrosslinked via UV light exposure to achieve dual crosslinking, forming both hydrogen and covalent bonds, to ensure long-term stability during multi-layer printing.

The analysis of printed simple one-layered lines with a target filament width of 0.25 mm provides insights into the bioink's print fidelity, consistency, and ability to maintain structure during extrusion and after deposition. Photographs in Fig. 6A show the printing outcomes of the control ink. Pluronic and HAMA-GA ink after 15 min (HAMA-GA, 15 min) or over 30 min (HAMA-GA, 30 min) of temporal oxidation at pH 5.5. Mean line length (Fig. 6C) and filament width (Fig. 6D) were measured to evaluate the dimensional accuracy [37]. The similarity of the printed Pluronic line length construct with the intended length of 20 mm revealed its highly printable properties (Fig. 6C). Furthermore, although Pluronic's filament width was considerably wider than the nozzle size, it was still closer to the nozzle diameter than the HAMA-GA inks. Pluronic also produces smooth filaments with a consistent width, and its Pr ′ 1 indicates perfectly square-shaped pores and, hence, ideal printability.

As expected, HAMA-GA at pH 5.5 without incubation (= without temporal oxidation) failed to produce fibers and started to spread during deposition on the printing substrate. This spreading occurs because the oxidative crosslinking has not yet had sufficient time to form. With shorter incubation times, the filament tended to spread after printing due to insufficient crosslinking. In contrast, longer incubation times resulted in excessive crosslinking, leading to irregular filament formation. The HAMA-GA ink at pH 5.5 began to form smooth fibers after mixing for 15 min, leading to a Pr-value of 0.85, which indicates the fusion of stacked filament layers due to inadequate cross-linking. Its rather smooth filaments also swell remarkedly, leading to a major deviation of the filament width from the nozzle diameter and longer filament lengths than Pluronic or HAMA-GA, 30 min.

After 30 min of mixing, the HAMA-GA at pH 5.5 ink underwent temporal oxidative crosslinking but could still be printed. The filament length was similar to Pluronic, and the filament width was closer to the nozzle size and control ink than that of the HAMA-GA, 15 min. However, HAMA-GA, 30 min, produces filament with a rough surface owing to over-gelling of the material. This finding is also supported by the printability evaluation achieved by analyzing the pore circularity of two-layer grids (Fig. 6B). The printability value (Pr) of HAMA-GA, 30 min, was Pr = 1.1, which suggests that the gel produces irregular pores and, hence, irregular filaments. As time passed, the ink transitioned slowly to a gel state on account of oxidative crosslinking and could not be extruded from the nozzle anymore.

These findings demonstrate that the temporal oxidation of HAMA-GA improves its printability and dimensional accuracy, with over 30 min of oxidation yielding better structural fidelity compared to 15–30 min, though challenges such as over gelation and filament irregularities remain. An incubation time of 15–30 min provides a very short printability window, which may compromise an optimal balance between

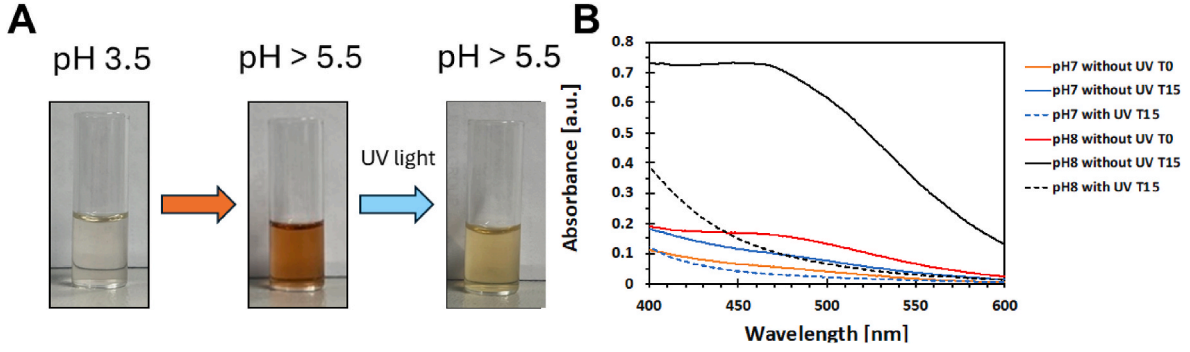

Fig. 4. The illustration of how photocrosslinking inhibits oxidative crosslinking through the radical quenching effect. (A) The color bleaching was observed after UV light exposure of oxidized gallol moiety. (B) UV–vis spectra of photo-inhibition effect in HAMA-GA samples at pH 7 and 8 before and after UV light exposure.

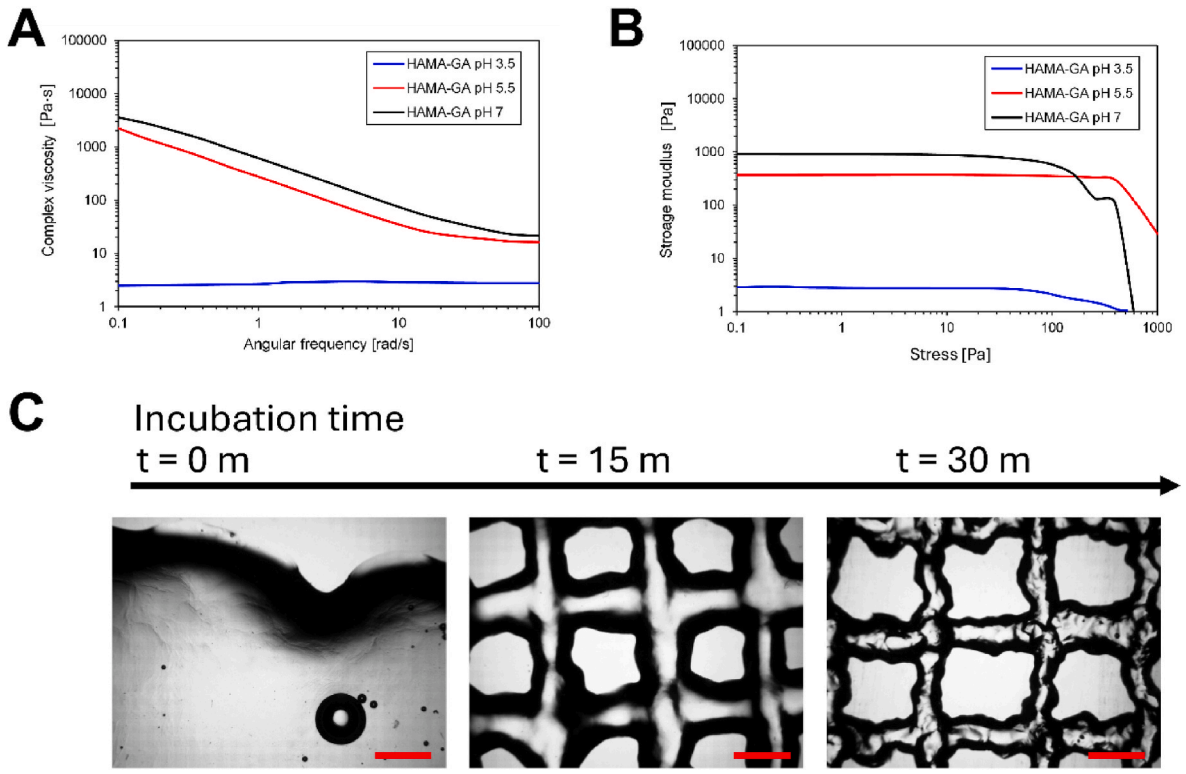

Fig. 5. Flow behavior and 3D printing of HAMA-GA inks. (A) The flow curves and storage moduli of the HAMA-GA biomaterial ink at pH 3.5, 5.5 and 7. (B) The storage moduli of HAMA-GA ink at pH 3.5, 5.5 and 7 (C) The time-dependent printability window for HAMA-GA at pH 5.5 was established by printing the ink into two-layered grid structures (0, 15 and 30 min). At t = 0, immediate swelling of the filaments was observed after printing; at t = 15, the filaments were smooth; and at t = 30, the filaments became irregular. Scale bars = 1 mm.

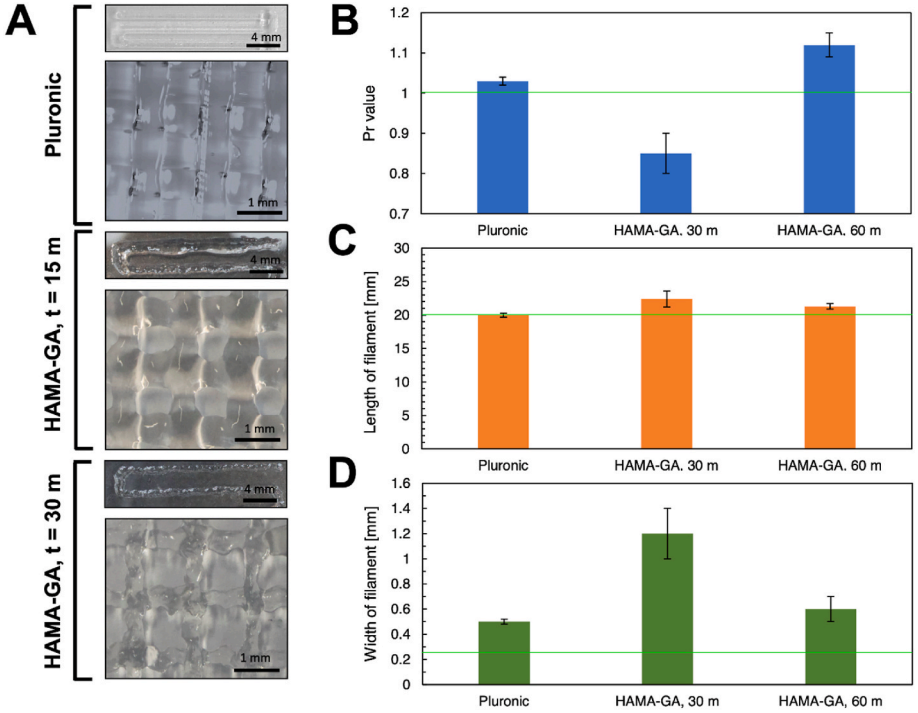

Fig. 6. The time-dependent printability window after 15 or 30 min of temporal oxidation was established for HAMA-GA at pH 5.5. (A) Printed single filaments and two-layered grid structures of Pluronic control ink and HAMA-GA ink after different oxidation times. (B) Printability (Pr) values of inks, (C) measured length of printed filaments and (D) measured filament widths. Scale bars either 1 mm or 4 mm.

achieving sufficient crosslinking and maintaining smooth, consistent filaments for enhanced printability.

Cohesive and adhesive properties of dual crosslinking HAMA-GA In general, the incorporation of gallol moieties enhances tissue adhesiveness of hydrogels, particularly when triggered under basic pH conditions [18]. This phenomenon is observed in the mussel byssus, known for its wet adhesion to the rock surfaces in marine environments. The suitability of catechol chemistry at a pH ≈ 8 aligns with the slightly alkaline nature of seawater, thereby improving adhesion in such conditions [38]. In previous studies [17,18], gallol-modified HA alone exhibited adhesive strength ranging from approximately 1 to 1.5 kPa, due to the presence of gallol groups. These groups mimic the adhesive proteins found in mussel foot proteins, such as 3,4dihydroxyphenylalanine (DOPA), which is a type of catechol [38,39]. In addition, several researchers have enhanced the wet adhesive strength by mixing catechol-containing groups with polymers containing free amino groups, such as chitosan and gelatin [11,12,40,41]. However, enhancing interfacial adhesion may compromise the cohesive force within the hydrogel because the gallol moieties reacts with the free amino group in the same polymers [42], leading to detachment over time [43].

In this study, our formulation involved modifying HA with methacrylate groups to enable photocrosslinking to enhance adhesive strength and cohesive force. The adhesive strength is attributed to the interaction between the gallol moieties and surfaces containing free amino groups, such as tissue. Oscillatory measurements, including amplitude and frequency sweeps, were conducted to assess the enhancement of viscoelasticity in HAMA-GA resulting from the quenching of oxidative crosslinking by exposure to the UV light. Fig. 7A shows that HAMA-GA hydrogel samples with plain oxidative crosslinking immediately lost their storage moduli, resulting in the samples escaping from the geometry; perhaps on account of *o*-quinone formation. This is observed by the sudden drop in storage modulus value with increasing strain. On the other hand, dual crosslinked HAMA-GA hydrogels through oxidative crosslinking and photocrosslinking maintained their integrity and exhibited a gradual decrease in storage modulus with increasing strain. The frequency sweep measurement further confirmed the viscoelastic behavior of both hydrogel samples, exhibiting gel-like behavior observed by increased storage and loss modulus as the frequency increased, as shown in Fig. 7B.

To measure wet adhesive strength, a tack test was conducted using a rotational rheometer at different pH values (3.5, 5.5 and 7). HAMA-GA samples at pH 3.5 exhibited the lowest adhesive strength and storage modulus because oxidative crosslinking only initiates at pH 5.5 or above, resulting in insufficient crosslinking in contrast to HAMA-GA at pH 5.5 and 7 (Fig. 7C and D). On the other hand, the adhesive strength significantly improved from 0.12 ± 0.01 to 4.4 ± 0.3 kPa at pH 3.5 after photocrosslinking, while at pH 5.5, it improved from 0.56 ± 0.01 to 6.4 ± 0.3 kPa. The improvement in adhesive strength was derived from the additional formation of oxidative crosslinking and the gallol–amine synergistic interaction between hydrogels and tissues enhances the adhesiveness at pH 5.5, which were further crosslinked by UV light exposure. In contrast, HAMA-GA hydrogels at pH 7 maintained the same adhesive strength as the sample at pH 5.5. However, the adhesive strength of the dual crosslinked hydrogel at pH 7 significantly decreased because the formation of *o*-quinone during oxidative crosslinking disrupted radical polymerization, including photocrosslinking [25,31]. Even though the adhesive strength of dual crosslinking in HAMA-GA improved, the storage modulus was reduced compared to the gels at pH 3.5. In addition, the adhesive strength of pH 3.5 was less than at pH 5.5 because of an increase in the cohesive force, which was 3.8 ± 0.1 and 4.9 ± 0.3 kPa, respectively [44]. To better understand the properties of the hydrogels, a swelling test was conducted over 15 days (Figure S-4). Upon immersion in DPBS, all hydrogels initially absorbed the solution and then gradually began to dissolve by day 3. As anticipated, on account of oxidative crosslinking, gallol-modified HA alone (HAGA) began to degrade and lost its structure throughout the observation period due to the instability of the oxidative crosslinking under aqueous conditions, whereas HAMA remained stable. Oxidative crosslinking, which relies on the formation of covalent bonds between gallol moieties, is susceptible to disruption when exposed to water, leading to the breakdown of the hydrogel network. Notably, HAMA-GA absorbed the solution, swelling up to 3–4 times its original size over the first 7 days, after which it began to shrink gradually over time. The higher swelling ratio observed in the dual-crosslinked HAMA-GA hydrogel compared to HAMA alone is attributed to the presence of gallol moieties, which increase water retention due to their hydrophilic and dynamic nature. This does not directly indicate a lower crosslinking density, as the covalent network formed via photocrosslinking provides mechanical stability, while gallol oxidation enhances viscoelasticity and hydration. Therefore, the incorporation of gallol groups has also been reported to minimize shrinkage in collagen-based hydrogels, which is beneficial for maintaining dimensional stability in tissue engineering applications,

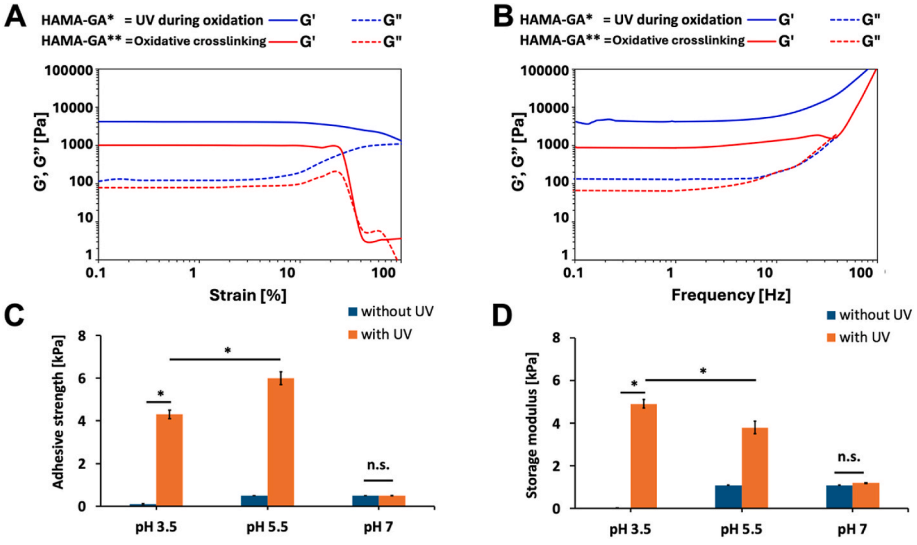

Fig. 7. Cohesive and adhesive properties of HAMA-GA with and without dual crosslinking. (A) Viscoelasticity of HAMA-GA with amplitude sweep at pH 5.5, (B) Viscoelasticity of HAMA-GA with frequency sweep at pH 5.5, (C) Wet adhesive strength under different pH conditions (3.5, 5.5, and 7), and (D) Storage moduli under different pH conditions (3.5, 5.5, and 7). A Student's t-test was conducted to determine statistical significance, with n.s. indicating not significant, and * representing significant with $p < 0.01$.

which is reported in previous literatures, where gallol or catechol groups enhance water retention [11] and promote stimuli responsiveness in hydrogels [18]. Therefore, the combined crosslinking mechanisms in HAMA-GA hydrogels offer a balance of mechanical integrity, viscoelasticity, and swelling capacity suitable for bioprinting and hydrogel fabrication.

Bioprinting and cytocompatibility of HAMA-GA bioinks We exploited the oxidative crosslinking properties of HAMA-GA to enable the printability at pH 5.5. Extrusion-based 3D bioprinting was performed to print cell-laden bioprinted constructs, which were subsequently cultured for 4 days. Fibroblasts, which are present in all connective tissues, were used as the standard model for cell viability analysis [45]. Bioink formulations were prepared at three pH levels: 3.5, 5.5, and 7.0. Although the precursor solutions were prepared under mildly acidic conditions (pH 3.5 and 5.5), the final formulations were neutralized upon 1:1 mixing with cell suspension in DMEM. Additionally, full medium exchange post-crosslinking further restored physiological conditions. This is consistent with the literatures where short-term exposure to acidic precursors did not compromise cell viability or spreading [46,47]. As mentioned in the previous section, pH 3.5 resulted in insufficient oxidative crosslinking; therefore, hydrogels were fabricated by casting instead of printing. In contrast, pH 5.5 hydrogels exhibited an optimal balance of crosslinking kinetics and mechanical integrity, allowing successful extrusion-based bioprinting. At pH 7.0, hydrogels underwent rapid oxidative crosslinking, which limited their printability and caused nozzle clogging; therefore, hydrogel fabrication was also performed using the casting method [12].

To evaluate the influence of pH on mechanical properties of hydrogels and cell behavior, we assessed storage modulus (G′) and stress relaxation profiles of hydrogels prepared at pH 3.5, 5.5 and 7 on Day 1 and Day 4, as shown in Fig. 8. In general, all groups exhibited a decreasing in G′ over 4 days, indicating the swelling and softening in hydrogel matrix during incubation (Fig. 8A). Hydrogels prepared at 3.5 demonstrated highest storage moduli (G' ≈ 8500 Pa), whereas hydrogels at pH 5.5 and pH 7 exhibited lower initial storage moduli (~3000–4000 Pa). At Day 4, G′ decreased for all formulations, but the pH 7 hydrogel exhibited the highest storage modulus, suggesting that the oxidative crosslinking still occurred overtime. The stress relaxation analysis further provides more insightful of viscoelastic behavior of hydrogels (Fig. 8B). The hydrogel at pH 3.5 exhibited high normalized stress over the observation period, indicating poor stress relaxation due to insufficient oxidative crosslinking, where photocrosslinking alone dominated the gelation process. On the other hand, both pH 5.5 and pH 7 hydrogels dissipated stress more efficiently, suggesting more dynamic and cell-responsive environments [48].

To further assess the mechanical properties and cytocompatibility of the hydrogels, experiments were conducted using both casting and printing methods with HAMA-GA formulations. First, we evaluated the acute effects on encapsulated cells within hydrogels exhibiting different stress relaxation profiles at pH 3.5, 5.5, and 7.0. For the pH 3.5 and pH 7.0 bioinks, the cell-laden bioinks were extruded through a printing nozzle into 12-well plates and photocrosslinked to encapsulate the cells within the hydrogels. For the pH 5.5 bioink, the cell-laden bioink was printed directly into 12-well plates and then crosslinked. Cell viability was subsequently assessed using a live/dead assay on Days 1 and 4 (Fig. 8C and D). Among all bioink formulations, only the pH 5.5 formulation exhibited sufficient oxidative crosslinking kinetics and rheological characteristics to support extrusion-based bioprinting. To evaluate the cellular response within different hydrogel formulations, cell viability was assessed over 4 days of culture. On Day 1, cells encapsulated in the pH 3.5 hydrogel exhibited the lowest viability (~40–45 %), with most cells appearing rounded, consistent with a stiffer, less-relaxing matrix environment. In contrast, both pH 5.5 (printed structure) and pH 7 (casted structure) supported higher initial viability, with values of approximately 70 % and 80 %, respectively, and more evident cell spreading. By Day 4, viability improved across all groups, and cells in all conditions transitioned from a rounded morphology to a more spread phenotype. Among the groups, the pH 5.5 printed hydrogel showed the most extensive cell spreading by Day 4. Despite the initial acidic conditions of some precursor solutions, cell viability remained high across all groups, indicating that the 1:1 mixing with buffered DMEM and post-gelation medium exchange effectively maintained cytocompatibility. This trend is consistent with its moderate initial stiffness, rapid stress relaxation behavior, and suitability for extrusion-based bioprinting [49].

4. Conclusion

Our work utilized pH-responsive viscosity modulation and triggered photocrosslinking in gallol-modified hyaluronic acid (HAMA-GA)

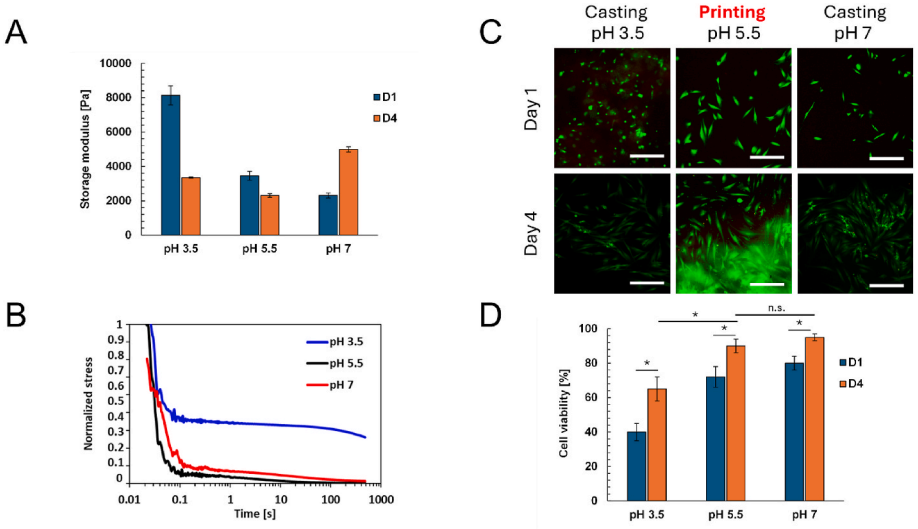

Fig. 8. Effect of pH on viscoelastic properties of HAMA-GA and cell viability on Day 1 and Day4 (A) G′ of hydrogels at pH 3.5, 5.5, and 7 on Day 1 and Day 4 (B) Stress relaxation behavior of hydrogels across different pH conditions, with pH 5.5 and 7 (C) Live/dead staining and quantified cell viability of hydrogels at pH 3.5, 5.5, and 7 on Day 1 and Day 4. Hydrogels were fabricated via casting (pH 3.5, 7) and printing (pH 5.5). Green: live cells; red: dead cells. Data are shown as mean ± SD (n = 3). $p < 0.05$ was considered significant. * = Day 4 vs Day 1 within the same pH; additional significance between groups is indicated. (D) Quantified cell viability on Day 1 and Day 4.

biomaterial inks, enabling control over temporal properties that directly influence the printability. We found that at pH 5.5, HAMA-GA exhibited optimal shear-thinning behavior and printability, while higher pH levels resulted in immediate gelation unsuitable for bioprinting. Post-printing photocrosslinking significantly enhanced the stability and adhesive strength of the printed scaffolds by quenching the oxidation process and reducing brittleness. This dual crosslinking strategy effectively combines oxidative and photocrosslinking mechanisms, improving the cohesive and adhesive properties of the hydrogels. Lastly, the results also demonstrate that hydrogel formulations tuned at pH 5.5 provide an optimal balance of printability, viscoelasticity, and mechanical support for cell viability. In summary, the pH-responsive viscosity modulation and two-step crosslinking approach ensure stable, bioprintable hydrogels, providing a versatile platform for developing a diverse library of bioinks for tissue engineering and regenerative medicine applications.

CRediT authorship contribution statement

Hatai Jongprasitkul: Writing – review & editing, Writing – original draft, Visualization, Validation, Project administration, Methodology, Investigation, Formal analysis, Data curation, Conceptualization. **Sanna Turunen:** Writing – review & editing, Writing – original draft, Visualization, Validation. **David A. Fulton:** Writing – review & editing, Writing – original draft. **Minna Kellomäki:** Writing – review & editing, Resources, Project administration, Funding acquisition. **Vijay Singh Parihar:** Writing – review & editing, Visualization, Validation, Supervision, Project administration, Methodology, Investigation, Formal analysis, Data curation, Conceptualization.

Declaration of competing interest

The authors declare that they have no known competing financial interests or personal relationships that could have appeared to influence the work reported in this paper.

Acknowledgment

The authors are grateful to The Centre of Excellence in Body-on-Chip Research (CoEBoC) by the Academy of Finland, Finland for financial support (decision #312409, #326587 and #336663) and to the Tampere University funding for the CoEBoC consortium.

Appendix A. Supplementary data

Supplementary data to this article can be found online at https://doi.org/10.1016/j.bprint.2025.e00432.

Data availability

Data will be made available on request.

References

[1] D. Shopova, A. Yaneva, D. Bakova, A. Mihaylova, P. Kasnakova, M. Hristozova, Y. Sbirkov, V. Sarafian, M. Semerdzhieva, (Bio)printing in personalized medicine—opportunities and potential benefits, Bioengineering 10 (2023) 287, https://doi.org/10.3390/BIOENGINEERING10030287, 2023, Vol. 10, Page 287.
[2] Z. Gu, J. Fu, H. Lin, Y. He, Development of 3D bioprinting: from printing methods to biomedical applications, Asian J. Pharm. Sci. 15 (2020) 529–557, https://doi.org/10.1016/J.AJPS.2019.11.003.
[3] P.S. Gungor-Ozkerim, I. Inci, Y.S. Zhang, A. Khademhosseini, M.R. Dokmeci, Bioinks for 3D bioprinting: an overview, Biomater. Sci. 6 (2018) 915, https://doi.org/10.1039/C7BM00765E.
[4] A. Zennifer, S. Manivannan, S. Sethuraman, S.G. Kumbar, D. Sundaramurthi, 3D bioprinting and photocrosslinking: emerging strategies & future perspectives, Biomater. Adv. 134 (2022) 112576, https://doi.org/10.1016/J.MSEC.2021.112576.
[5] P. Bertsch, M. Diba, D.J. Mooney, S.C.G. Leeuwenburgh, Self-healing injectable hydrogels for tissue regeneration, Chem. Rev. 123 (2023) 834–873, https://doi.org/10.1021/acs.chemrev.2c00179.
[6] J. Manasi Esther, R. Solanki, M. Dhanka, P. Thareja, D. Bhatia, Self-healing, injectable chitosan-based hydrogels: structure, properties and biological applications, Mater. Adv. 5 (2024) 5365–5393, https://doi.org/10.1039/D4MA00131A.
[7] M.K. Włodarczyk-Biegun, J.I. Paez, M. Villiou, J. Feng, A. Del Campo, Printability study of metal ion crosslinked PEG-Catechol based inks, Biofabrication 12 (2020) 035009, https://doi.org/10.1088/1758-5090/ab673a.
[8] W. Zhang, R. Wang, Z.M. Sun, X. Zhu, Q. Zhao, T. Zhang, A. Cholewinski, F. Yang, B. Zhao, R. Pinnaratip, P.K. Forooshani, B.P. Lee, Catechol-functionalized hydrogels: biomimetic design, adhesion mechanism, and biomedical applications, Chem. Soc. Rev. 49 (2020) 433, https://doi.org/10.1039/C9CS00285E.
[9] A. Andersen, M. Krogsgaard, H. Birkedal, Mussel-inspired self-healing double-cross-linked hydrogels by controlled combination of metal coordination and covalent cross-linking, Biomacromolecules 19 (2018) 1402–1409, https://doi.org/10.1021/acs.biomac.7b01249.
[10] K. Kaniewska, P. Kościelniak, M. Karbarz, pH modulated formation of complexes with various stoichiometry between polymer network and Fe(III) in thermosensitive gels modified with gallic acid, Gels 9 (2023) 447, https://doi.org/10.3390/gels9060447, 2023, Vol. 9, Page 447.
[11] M. Shin, H. Lee, Gallol-rich hyaluronic acid hydrogels: shear-thinning, protein accumulation against concentration gradients, and degradation-resistant properties, Chem. Mater. 29 (2017) 8211–8220, https://doi.org/10.1021/acs.chemmater.7b02267.
[12] M. Shin, J.H. Galarraga, M.Y. Kwon, H. Lee, J.A. Burdick, Gallol-derived ECM-Mimetic adhesive bioinks exhibiting temporal shear-thinning and stabilization behavior, Acta Biomater. 95 (2019) 165–175, https://doi.org/10.1016/j.actbio.2018.10.028.
[13] G. Bovone, O.Y. Dudaryeva, B. Marco-Dufort, M.W. Tibbitt, Engineering hydrogel adhesion for biomedical applications via chemical design of the junction, ACS Biomater. Sci. Eng. 7 (2021) 4048–4076, https://doi.org/10.1021/acsbiomaterials.0c01677.
[14] M.A. Gwak, Y. Hyeok Choi, M. Hee Kim, W. Ho Park, Mussel byssus-inspired gallol-enriched chitosan hydrogel fibers with strong adhesive properties, Eur. Polym. J. 204 (2024) 112673, https://doi.org/10.1016/J.EURPOLYMJ.2023.112673.
[15] M.A. Gwak, S.J. Lee, D. Lee, S.A. Park, W.H. Park, Highly gallol-substituted, rapidly self-crosslinkable, and robust chitosan hydrogel for 3D bioprinting, Int. J. Biol. Macromol. 227 (2023) 493–504, https://doi.org/10.1016/J.IJBIOMAC.2022.12.124.
[16] A. Mörö, S. Samanta, L. Honkamäki, V.K. Rangasami, P. Puistola, M. Kauppila, S. Narkilahti, S. Miettinen, O. Oommen, H. Skottman, Hyaluronic acid based next generation bioink for 3D bioprinting of human stem cell derived corneal stromal model with innervation, Biofabrication 15 (2023) 015020, https://doi.org/10.1088/1758-5090/acab34.
[17] H. Jongprasitkul, S. Turunen, M. Kellomäki, V.S. Parihar, A comprehensive study on rheological properties of photocrosslinkable gallol-metal complexed hyaluronic acid-based biomaterial inks, Mater. Adv. 5 (2024) 5823–5837, https://doi.org/10.1039/D4MA00273C.
[18] H. Jongprasitkul, V.S. Parihar, S. Turunen, M. Kellomäki, pH-Responsive gallol-functionalized hyaluronic acid-based tissue adhesive hydrogels for injection and three-dimensional bioprinting, ACS Appl. Mater. Interfaces (2023), https://doi.org/10.1021/acsami.3c02961.
[19] H. Jongprasitkul, S. Turunen, V.S. Parihar, M. Kellomäki, Two-step crosslinking to enhance the printability of methacrylated gellan gum biomaterial ink for extrusion-based 3D bioprinting, Bioprinting 25 (2022) e00185, https://doi.org/10.1016/j.bprint.2021.e00185.
[20] H. Jongprasitkul, S. Turunen, V.S. Parihar, M. Kellomäki, Sequential cross-linking of gallic acid-functionalized GelMA-Based bioinks with enhanced printability for extrusion-based 3D bioprinting, Biomacromolecules 24 (2023) 502–514, https://doi.org/10.1021/acs.biomac.2c01418.
[21] H. Jongprasitkul, S. Turunen, V.S. Parihar, S. Annurakshita, M. Kellomaki, Photocross-linkable methacrylated polypeptides and polysaccharides for casting, injecting, and 3D fabrication, Biomacromolecules 22 (2021) 481–493, https://doi.org/10.1021/acs.biomac.0c01322.
[22] N. Paxton, W. Smolan, T. Böck, F. Melchels, J. Groll, T. Jungst, Proposal to assess printability of bioinks for extrusion-based bioprinting and evaluation of rheological properties governing bioprintability, Biofabrication 9 (2017) 44107, https://doi.org/10.1088/1758-5090/aa8dd8.
[23] F. Perin, E. Spessot, A. Famà, A. Bucciarelli, E. Callone, C. Mota, A. Motta, D. Maniglio, Modeling a dynamic printability window on polysaccharide blend inks for extrusion bioprinting, ACS Biomater. Sci. Eng. 9 (2023) 1320–1331, https://doi.org/10.1021/acsbiomaterials.2c01143.
[24] L. Ouyang, R. Yao, Y. Zhao, W. Sun, Effect of bioink properties on printability and cell viability for 3D bioplotting of embryonic stem cells, Biofabrication 8 (2016) 1–12, https://doi.org/10.1088/1758-5090/8/3/035020.
[25] H. Montazerian, S. Mitra, A. Hassani Najafabadi, R. Seyedmahmoud, Y. Zheng, M. R. Dokmeci, N. Annabi, A. Khademhosseini, P.S. Weiss, Catechol conjugation for bioadhesion in photo-cross-linkable biomaterials, ACS Mater. Lett. 5 (2023) 1672–1683, https://doi.org/10.1021/acsmaterialslett.3c00193.
[26] L. Koivusalo, M. Kauppila, S. Samanta, V.S. Parihar, T. Ilmarinen, S. Miettinen, O. P. Oommen, H. Skottman, Tissue adhesive hyaluronic acid hydrogels for sutureless stem cell delivery and regeneration of corneal epithelium and stroma, Biomaterials 225 (2019) 119516, https://doi.org/10.1016/j.biomaterials.2019.119516.
[27] G.R. Park, M.A. Gwak, Y.H. Choi, W.H. Park, pH-sensitive gallol-rich chitosan hydrogel beads for on-off controlled drug delivery, Int. J. Biol. Macromol. 240 (2023) 124346, https://doi.org/10.1016/J.IJBIOMAC.2023.124346.

[28] P.K.M. Adnan, L. Sreejith, Compact poly-electrolyte complex hydrogels of gelatin and sodium alginate for sensing wound status, Mater. Lett. 313 (2022) 131705, https://doi.org/10.1016/J.MATLET.2022.131705.
[29] S. Samanta, V.K. Rangasami, H. Sarlus, J.R.K. Samal, A.D. Evans, V.S. Parihar, O. P. Varghese, R.A. Harris, O.P. Oommen, Interpenetrating gallol functionalized tissue adhesive hyaluronic acid hydrogel polarizes macrophages to an immunosuppressive phenotype, Acta Biomater. 142 (2022) 36–48, https://doi.org/10.1016/j.actbio.2022.01.048.
[30] S. Samanta, V.K. Rangasami, N.A. Murugan, V.S. Parihar, O.P. Varghese, O. P. Oommen, An unexpected role of an extra phenolic hydroxyl on the chemical reactivity and bioactivity of catechol or gallol modified hyaluronic acid hydrogels, Polym. Chem. 12 (2021) 2987–2991, https://doi.org/10.1039/d1py00013f.
[31] J. Lee, K. Chang, S. Kim, V. Gite, H. Chung, D. Sohn, Phase controllable hyaluronic acid hydrogel with iron(III) ion-catechol induced dual cross-linking by utilizing the gap of gelation kinetics, Macromolecules 49 (2016) 7450–7459, https://doi.org/10.1021/acs.macromol.6b01198.
[32] D.G. Barrett, D.E. Fullenkamp, L. He, N. Holten-Andersen, K.Y.C. Lee, P. B. Messersmith, pH-Based regulation of hydrogel mechanical properties through mussel-inspired chemistry and processing, Adv. Funct. Mater. 23 (2013) 1111–1119, https://doi.org/10.1002/adfm.201201922.
[33] R. Song, X. Wang, M. Johnson, C. Milne, A. Lesniak-Podsiadlo, Y. Li, J. Lyu, Z. Li, C. Zhao, L. Yang, I. Lara-Sáez, A. Sigen, W. Wang, Enhanced strength for double network hydrogel adhesive through cohesion-adhesion balance, Adv. Funct. Mater. 34 (2024) 2313322, https://doi.org/10.1002/ADFM.202313322.
[34] J.T. Lin, H.W. Liu, K.T. Chen, D.C. Cheng, Modeling the optimal conditions for improved efficacy and crosslink depth of photo-initiated polymerization, Polymers 11 (2019), https://doi.org/10.3390/POLYM11020217.
[35] K.S. Lim, B.S. Schon, N.V. Mekhileri, G.C.J. Brown, C.M. Chia, S. Prabakar, G. J. Hooper, T.B.F. Woodfield, New visible-light photoinitiating system for improved print fidelity in gelatin-based bioinks, ACS Biomater. Sci. Eng. 2 (2016) 1752–1762, https://doi.org/10.1021/acsbiomaterials.6b00149.
[36] K. Phan, E.E. Lessard, J.A. Reed, M.G. Warsen, S. Zimmer, L.M. Landino, Concurrent photooxidation and photoreduction of catechols and para-quinones by chlorophyll metabolites, Photochemistry 4 (2024) 346–360, https://doi.org/10.3390/photochem4030021.
[37] K.V. Balaji, S. Bhutoria, S. Nayak, P. Anil Kumar, S. Velayudhan, Printability assessment of modified filament deposition modelling three dimensional bioprinter printer using polymeric formulations, Biomedical Engineering Advances 5 (2023) 100083, https://doi.org/10.1016/J.BEA.2023.100083.
[38] N. Holten-Andersen, M.J. Harrington, H. Birkedal, B.P. Lee, P.B. Messersmith, K. Yee, C. Lee, J.H. Waite, pH-induced metal-ligand cross-links inspired by mussel yield self-healing polymer networks with near-covalent elastic moduli, (n.d.). https://doi.org/10.1073/pnas.1015862108/-/DCSupplemental.
[39] N. Holten-Andersen, A. Jaishankar, M.J. Harrington, D.E. Fullenkamp, G. Dimarco, L. He, G.H. McKinley, P.B. Messersmith, K.Y.C. Lee, Metal-coordination: using one of nature's tricks to control soft material mechanics, J. Mater. Chem. B 2 (2014) 2467–2472, https://doi.org/10.1039/c3tb21374a.
[40] M. Marzano, N. Borbone, F. Amato, G. Oliviero, P. Fucile, T. Russo, F. Sannino, 3D chitosan-gallic acid complexes: assessment of the chemical and biological properties, Gels 8 (2022) 124, https://doi.org/10.3390/GELS8020124/S1.
[41] M. Xie, B. Hu, Y. Wang, X. Zeng, Grafting of gallic acid onto chitosan enhances antioxidant activities and alters rheological properties of the copolymer, J. Agric. Food Chem. 62 (2014) 9128–9136, https://doi.org/10.1021/jf503207s.
[42] X. Peng, Y. Li, T. Li, Y. Li, Y. Deng, X. Xie, Y. Wang, G. Li, L. Bian, Coacervate-derived hydrogel with effective water repulsion and robust underwater bioadhesion promotes wound healing, Adv. Sci. 9 (2022) 2203890, https://doi.org/10.1002/ADVS.202203890.
[43] Y. Bu, A. Pandit, Cohesion mechanisms for bioadhesives, Bioact. Mater. 13 (2022) 105–118, https://doi.org/10.1016/J.BIOACTMAT.2021.11.008.
[44] B. Yang, C. Lim, D.S. Hwang, H.J. Cha, Switch of surface adhesion to cohesion by Dopa-Fe3+ complexation, in response to microenvironment at the mussel plaque/Substrate interface, Chem. Mater. 28 (2016) 7982–7989, https://doi.org/10.1021/acs.chemmater.6b03676.
[45] S.P. Pereira, C.M. Deus, T.L. Serafim, T. Cunha-Oliveira, P.J. Oliveira, Metabolic and phenotypic characterization of human skin fibroblasts after forcing oxidative capacity, Toxicol. Sci. 164 (2018) 191–204, https://doi.org/10.1093/toxsci/kfy068.
[46] A. Souza, M. Parnell, B.J. Rodriguez, E.G. Reynaud, Role of pH and crosslinking ions on cell viability and metabolic activity in alginate–gelatin 3D prints, Gels 9 (2023), https://doi.org/10.3390/gels9110853.
[47] G.V.N. Rathna, Gelatin hydrogels: enhanced biocompatibility, drug release and cell viability, J. Mater. Sci. Mater. Med. 19 (2008) 2351–2358, https://doi.org/10.1007/s10856-007-3334-9.
[48] A. Bauer, L. Gu, B. Kwee, W.A. Li, M. Dellacherie, A.D. Celiz, D.J. Mooney, Hydrogel substrate stress-relaxation regulates the spreading and proliferation of mouse myoblasts, Acta Biomater. 62 (2017) 82–90, https://doi.org/10.1016/j.actbio.2017.08.041.
[49] D.E. Discher, P. Janmey, Y.L. Wang, Tissue cells feel and respond to the stiffness of their substrate, Science 310 (2005) 1139–1143, https://doi.org/10.1126/SCIENCE.1116995, 1979.